03

Effects of degenerate light diffraction on a periodic domain structure in 1% MgO : $LiTaO_3$ in the temperature range of 30–110°C

© A.V. Dubikov[1], E.N. Savchenkov[1], D.E. Belskaya[1], S.M. Shandarov[1], N.I. Burimov[1], S.V. Smirnov[1], A.R. Akhmatkhanov[2], M.A. Chuvakova[2], V.Ya. Shur[2]

[1] Tomsk State University of Control Systems and Radioelectronics, Tomsk, Russia
[2] Ural Federal University after the first President of Russia B.N. Yeltsin, Yekaterinburg, Russia

e-mail: rossler@mail.ru

Received May 13, 2024
Revised June 06, 2024
Accepted June 13, 2024

The effects of degenerate anisotropic diffraction were observed for the first time on a periodic regular domain structure (RDS) formed in it with non-inclined Y-type walls for a probing beam with a wavelength of $\lambda = 632.8$ nm at temperatures below and above the isotropic point in a stoichiometric crystal of 1% MgO : $LiTaO_3$. The use of experimentally measured maximum efficiency values for two-fold degenerate diffraction processes with an unusual and ordinary probing beam made it possible to obtain an estimate of $|f_{1132} + f_{3131}| \approx 18$ V for the flexoelectric tensor components of the studied lithium tantalate sample. The temperature of the isotropic point $T_i = 69.31$°C was determined and the temperature dependences of birefringence $\delta n(T)$ in the range from 30 to 110°C were approximated from the analysis of experimental temperature dependences for the transmitted power through the 1% MgO : $LiTaO_3$ crystal and a crossed analyzer of a probing beam with a polarization vector oriented at an angle of 45° to the Z axis.

Keywords: lithium tantalate, degenerate diffraction, isotropic point, flexoelectric tensor component.

DOI: 10.61011/EOS.2024.07.59648.6267-24

Periodic, aperiodic and fan type regular domain structures (RDS) are currently addressed and studied experimentally as components enabling various effects of nonlinear optical laser transformations [1–10] and electrooptical parameter control [1,5,6,11,12] to be implemented. A stoichiometric ferroelectric lithium tantalate crystal doped with magnesium oxide (1% MgO : $LiTaO_3$), with the transmission region from 0.26 to $\sim 5.5\,\mu$m is an attractive material for creating RDS [1]. It should be noted that lengthwise variations of the RDS spatial period from the specified value defined by the quasi-synchronism conditions shall not exceed 20 nm [13]. For adapt to the quasi-synchronism conditions, temperature stabilization of the RDS components with accuracy ±0.05°C is used [2]. The operating temperature T may vary in a range from room temperature to 100°C [10] that contains an isotropic point with zero birefringence $\delta n(T) = n_e(T) - n_o(T)$ at $\lambda = 632.8$ nm for the undoped lithium tantalate [14]. However, for the stoichiometric 1% MgO : $LiTaO_3$ crystal, the Sellmeier equations provided in the existing literature to describe simultaneously the temperature and spectral dependences for the ordinary $(n_o(\lambda, T))$ [15] and extraordinary $(n_e(\lambda, T))$ [15–17] refractive indices poorly agree with each other.

The Bragg laser beam diffraction on disturbances of the optical properties of the ferroelectric crystal induced by the domain walls is an effective non-destructive test method used for quality control of periodically poled structures [18–23]. Mechanisms of these disturbances for uncharged walls are associated with spontaneous polarization variations within the walls and with induced elastic deformations due to electrostriction and inverse flexoelectric effect. For crystals of symmetry class 3m that includes lithium niobate (LN) and lithium tantalate (LT), distributions of elastic deformation tensor components $S_{kl}^{YZ}(x)$ and $S_{kl}^{XZ}(y)$ for the Y- and X-type walls, respectively, were obtained in the analytical form in [26] using the known domain wall model [24] and Helmholtz free energy expansion for a ferroelectric material with second-order phase transition taking into account the flexoelectric effect [25] contribution to the Helmholtz free energy. For RDS with the Y-walls, the presence of non-zero components $S_{13}^{YZ}(x) = S_{31}^{YZ}(x)$ and $S_{23}^{YZ}(x) = S_{32}^{YZ}(x)$ attributed to the inverse flexoelectric effect and electrostriction, respectively, as specified in [26] and earlier in [27], induces disturbances of optical properties due to the elastic-optical effect. These disturbances make it possible to implement the anisotropic Bragg diffraction in propagation of interacting ordinary and extraordinary light waves in the crystal's XY plane. Such anisotropic diffraction on RDS was experimentally observed at room temperature both in 5% MgO : $LiNbO_3$ [19,20,22] and 1% MgO : $LiTaO_3$ [22,23]. The Bragg conditions for the anisotropic diffraction on RDS in the 1% MgO : $LiTaO_3$ crystal that is observed in the first order at small angles between the probing beam and the Y axis[22] are defined by the temperature-dependent difference of squared refractive indices $n_o^2(T) - n_e^2(T)$, and diffraction efficiency is defined

by the dielectric tensor components $\Delta\varepsilon_{13}(x) = \Delta\varepsilon_{31}(x)$ associated with the flexoelectric coupling components f_{1132} and f_{3131} [26,27].

The anisotropic Bragg diffraction in linearly birefringent crystals is widely used in acousto-optic light control devices and is well studied [28,29]. In particular conditions, such crystals show light diffraction on monochromatic acoustic waves, where two or even three diffraction peaks occur together with zero peak [28–31]. It is degenerate by the Bragg condition [30], i.e by the acoustic wave vector. When two diffraction peaks arise and the Bragg conditions are simultaneously fulfilled for them, such diffraction is commonly referred to as the double diffraction [28,31]. This study first investigated the $\lambda = 632.8$ nm laser light anisotropic Bragg diffraction doubly degenerate by the RDS lattice vector. For RDS with Y-type non-sloping walls with the spatial period $\Lambda = 7.99\,\mu$m that is formed in the stoichiometric 1% MgO : $LiTaO_3$ crystal, implementation of this type of diffraction in the temperature range from 30 to 110°C containing the isotropic point at $T_i = 69.31$°C made it possible to approximate the temperature dependences of refractive indices $n_e(T)$ and $n_o(T)$ for this range, and to estimate possible values of the flexoelectric coupling tensor components f_{1132} and f_{3131}.

The experiments investigated RDS fabricated by Labfer company using the space-periodic electric field repolarization method [32] in the stoichiometric 1% MgO : $LiTaO_3$ crystal with dimensions $6.0 \times 1.9 \times 1.0$ mm^3 along the X, Y and Z axes, respectively. Observation of the isotropic and anisotropic Bragg diffraction and angular selectivity investigations [22,23] showed that RDS had Y-type non-sloping domain walls separating the original and repolarized crystal regions forming a bulk diffraction grating with the spatial period $\Lambda = 7.99\,\mu$m and effective dimension $d_{ef} = 1.85$ mm along the Y axis. Optical images of the sample's faces Z^+ and Z^- recorded using the Biolan microscope showed that dimensions of the original and repolarized RDS regions, h_i and $h_P = \Lambda - h_i$, respectively, differ from each other by $\Delta \approx 0.19\Lambda$ on average.

To implement the measurement temperature range from 10 to 110°C, RDS sample *1* was placed on Peltier element *2* in the experimental setup schematically illustrated in Figure 1. The Peltier element current was controlled using a stabilized DC voltage source. The sample temperature was controlled with 0.04°C increment using the readings of digital indicators *3* and *4* from two semiconductor temperature sensors *5* and *6* contacting the X-faces of the crystal and was calculated as a mean value at any time. The Peltier element *2* with the studied sample *1* was secured on a precision turntable used to change the angle position of RDS with respect to probing laser beam *7* from He–Ne-laser *8* with $\lambda = 632.8$ nm and to lock it with an accuracy of a minute of angle. The probing beam was formed in various experiments using spherical or cylindrical lenses with focal distances of 250 mm and 350 mm, respectively, from the original Gaussian beam with an aperture of 0.7 mm and a power of 22.5 mW such that its waist coincided

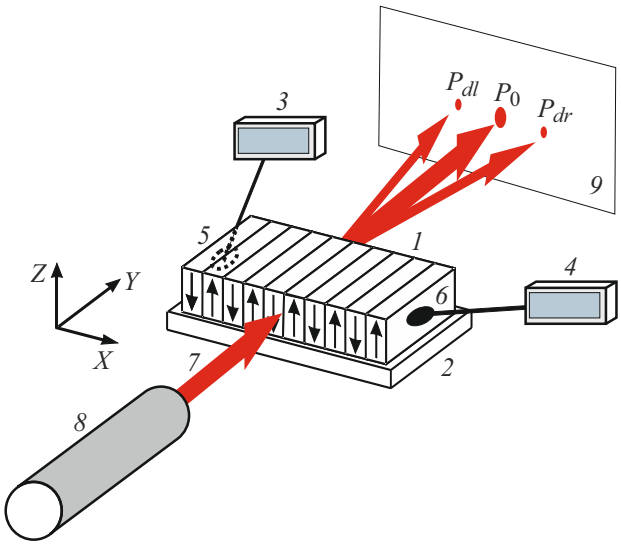

Figure 1. Experimental setup: *1* — 1% MgO : $LiTaO_3$ crystal with RDS with period 7.99 μm; *2* — Peltier element; *3* and *4* — temperature indicators; *5* and *6* — temperature sensors; *7* — probing laser beam; *8* — He–Ne-laser; *9* — screen.

with the middle (with respect to the z coordinate) of the inlet face $y = 0$. Laser beam polarization vector in various experiments was oriented along the crystallographic direction Z, in the XY plane or at 45° to the Z axis. Powers of the probing beam (P_0) and diffracted beam P_{dr} and P_{dl} (Figure. 1) were measured using the THORLABS-100D power meter. Qualitative view of the observed far-field diffraction patterns was displayed on screen *9* at a distance of $L = 1$ m from the crystal outlet face $y = d$ visually and using a digital camera.

The isotropic point with $\delta n(T_i) = 0$ at $T = T_i$ leads to two possible options of experimental observation of the doubly degenerate anisotropic Bragg diffraction on the RDS domain walls in the 1% MgO : $LiTaO_3$ crystal. Vector diagrams of the domain walls are illustrated in Figure 2.

To observe the degenerate diffraction below the isotropic point temperature (Figure 2, *a*), the extraordinary probing beam with the wave vector $\mathbf{k}_e$ shall propagate in the crystal orthogonally to the vector $\mathbf{K}$ corresponding to the first spatial harmonic of disturbances of the dielectric tensor components $\Delta\varepsilon_{13}(x) = \Delta\varepsilon_{31}(x)$ induced by the RDS domain walls. Such propagation direction of the probing beam was set experimentally by defining two angular positions of the turntable with the crystal at which the +1-st and −1-st order isotropic Bragg diffraction was observed on RDS as a mean value between the two positions. In this case the left peak (l) and right peak (r) corresponding to the ordinary waves and observed at the doubly degenerate Bragg diffraction at $T_{dgb} \approx 41.5$°C, the pattern of which is shown in Figure 3, *a*, are arranged symmetrically with respect to the peak for the probing beam (diffraction angle $\theta_{ol} = -\theta_{or}$), and their intensities are close to each other ($P_{dl} \approx P_{dr}$).

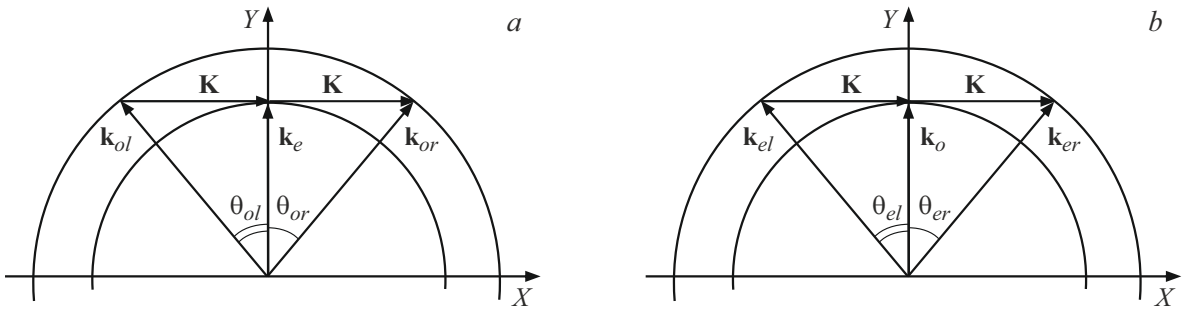

Figure 2. Vector diagrams of the doubly degenerate anisotropic Bragg diffraction on RDS in the 1% MgO : $LiTaO_3$ crystal at $T_{dgb} < T_i$ below the isotropic point for the extraordinary probing beam (a) and $T_{dgu} > T_i$ above the isotropic point for the ordinary probing beam (b).

Figure 3. Far-field patterns for the doubly degenerate anisotropic Bragg diffraction on the RDS domain walls ($\Lambda = 7.99\,\mu$m) in the 1% MgO : $LiTaO_3$ crystal: (a) — with $T_{dgb} = 41.5^\circ$C and the extraordinary probing beam, see the vector diagram in Figure 2, a; (b) — with $T_{dgu} = 91.5^\circ$C and the ordinary probing beam, see the vector diagram in Figure 2, b.

For the ordinary probing beam propagating in the crystal in the same direction as in the first case, the degenerate Bragg diffraction is observed at $T_{dgu} \approx 91.5^\circ$C and is described by the vector diagram illustrated in Figure 2, b. In this case, in the diffraction pattern shown in Figure 3, b, there are two symmetric peaks with similar intensities ($P_{dl} \approx P_{dr}$) corresponding to the extraordinary waves with vectors $\mathbf{k}_{er}$ and $\mathbf{k}_{el}$ that form with the probing wave vector $\mathbf{k}_o$ the angles θ_{er} and $\theta_{el} = -\theta_{er}$, respectively. Measured diffraction angles in air were close to the calculated values

$$\theta_{or}^{air}(T_{dgb}) = \theta_{er}^{air}(T_{dgu}) = \text{asin}(\lambda/\Lambda) = 0.0792\,\text{rad.},$$

corresponding to the vector diagrams shown in Figure 2, for implementation of which the following conditions shall be fulfilled

$$n_o^2(T_{dgb}) - n_e^2(T_{dgb}) = n_e^2(T_{dgu}) - n_o^2(T_{dgu}) = \left(\frac{\lambda}{\Lambda}\right)^2. \quad (1)$$

Thus, the difference of squared refractive indices of the 1% MgO : $LiTaO_3$ crystal at $\lambda = 632.8$ nm at T_{dgb} and T_{dgu} corresponding to the implementation of the doubly degenerate anisotropic Bragg diffraction on RDS with $\Lambda = 7.99\,\mu$m may be estimated from the experimental data as

$$n_o^2(T_{dgb}) - n_e^2(T_{dgb}) = n_e^2(T_{dgu}) - n_o^2(T_{dgu}) = 6.27 \cdot 10^{-3}.$$

Experimental dependences of the doubly degenerate Bragg diffraction efficiency measured with the ordinary and extraordinary probing beams in the temperature ranges from 35 to 47°C and from 86 to 99°C, respectively, are shown dotted in Figure 4.

To measure experimentally the temperature dependence of birefringence $\delta n(T) = n_o(T) - n_e(T)$ of the 1% MgO : $LiTaO_3$ crystal with RDS using the known procedure [14], the probing beam polarization vector was oriented at 45° to the Z axis. After transmission of this beam through a crystal with dimension$d = 1.9$ mm along the Y axis and the crossed analyzer, the THORLABS-100D meter measured the power-temperature dependence defined by the birefringence as

$$P(T) = P_0 \sin^2\left[\frac{\pi d}{\lambda}\,\delta n(T)\right]. \quad (2)$$

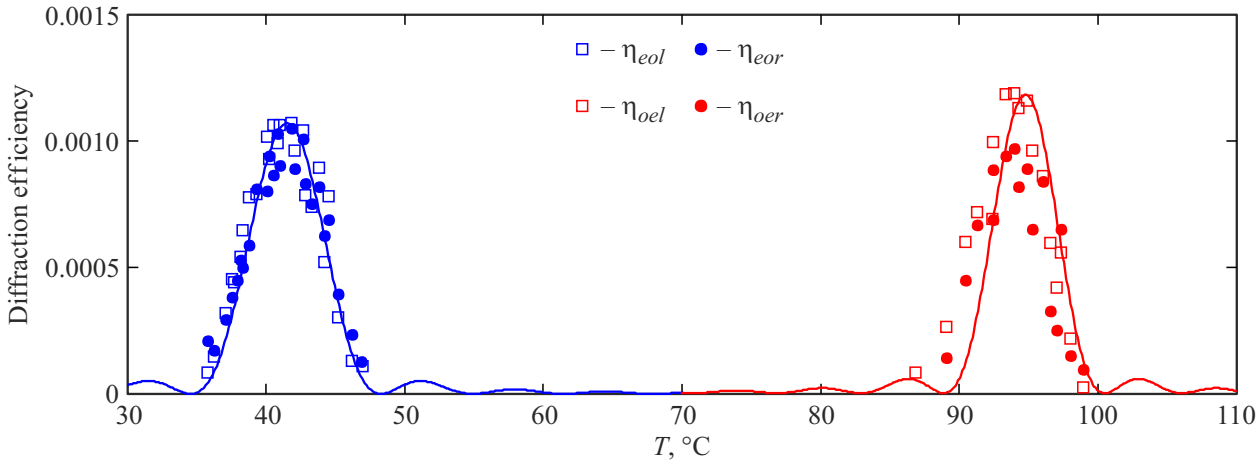

Figure 4. Temperature dependences of the efficiency of the doubly degenerate anisotropic Bragg diffraction on the RDS domain walls ($\Lambda = 7.99\,\mu$m) in the 1% MgO : LiTaO$_3$ crystal at $\Lambda = 632.8$ nm. Experimental points — for the left (η_{eol} and η_{oel}) and right (η_{eor} and η_{oer}) diffraction peaks with the extraordinary (eo, $T < T_i$) and ordinary (oe, $T > T_i$) probing beams; blue and red curves — calculation using equations (7), (6) and (10), (9), respectively.

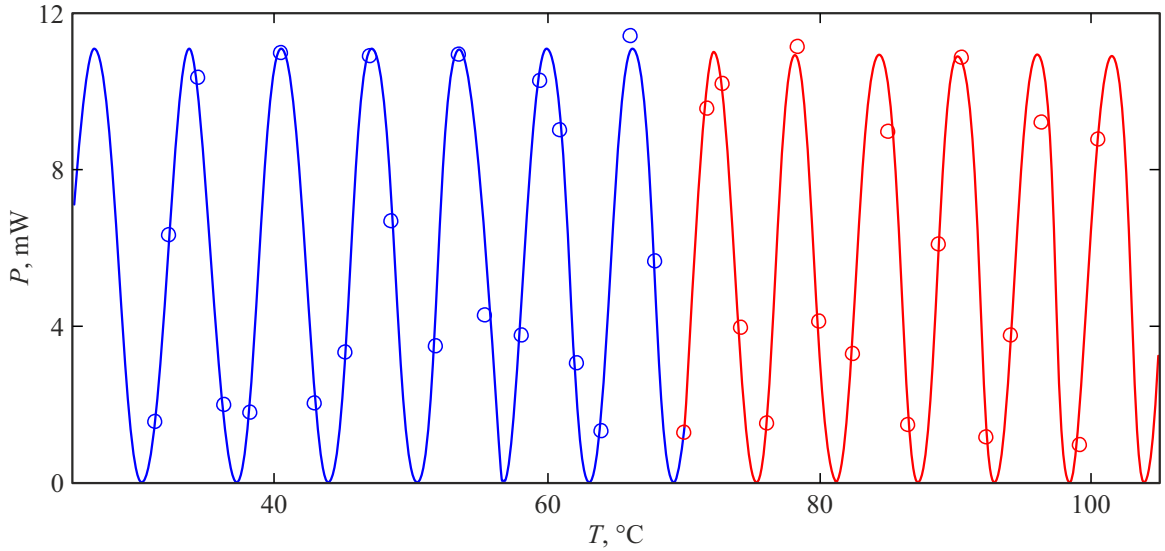

Figure 5. Temperature dependences for the power of the $\lambda = 632.8$ nm, 22.5 mW probing beam with the polarization vector oriented at 45° to the crystal's Z axis that was transmitted through the sample with RDS and crossed analyzer. Dots — experimental data; blue and red curves — calculation by equations (2) and (3) using the expansion coefficients A_{ib} and A_{iu}, respectively, as listed in the table.

The obtained results from the temperature range from 30 to 101°C are shown dotted in Figure 5.

Approximation of this experimental temperature dependence used the expansion of the functions $\delta n_b(T)$ (for $T \le T_i$) and $\delta n_u(T)$ (for $T \ge T_i$) as power series

$$\delta n_{b,u}(T) = A_{1b,1u}(T - T_i) + A_{2b,2u}(T - T_i)^2 + A_{3b,3u}(T - T_i)^3 + A_{4b,4u}(T - T_i)^4 \qquad (3)$$

and the least-square fitting procedure due to which the isotropic point temperature was measured as $T_i = 69.311$°C, and the expansion coefficients A_{ib} and A_{iu} whose values are listed in the table.

The measured isotropic point temperature for the studied sample differs from $T_i = (98.0 \pm 0.2)$°C for the undoped LiTaO$_3$ crystal containing 49.96% mol of Li$_2$O [14]. Moreover, the calculation using the Sellmeier equations described in [15] for the stoichiometric 1% MgO : LiTaO$_3$ crystal leads to $T_i = 94.17$°C. Thus differences may be associated with corresponding deviations from the stoichiometry of the compared crystals. Concentration of Li$_2$O in the studied 1% MgO : LiTaO$_3$ sample with $T_i = 69.311$°C estimated using the relations from [14] is equal to 49.79% mol.

Low efficiencies of the doubly degenerate anisotropic Bragg diffraction (Figure 4) allow the weak coupling approximation to be used for description of the temperature-

Expansion coefficients A_{ib} and A_{iu} for the temperature dependence of birefringence $\delta n_{b,u}(T) = n_0(T) - n_e(T)$ in the 1% MgO : $LiTaO_3$ crystal approximated by equation (3) below and above the isotropic point temperature, respectively

Expansion coefficients for $T \le T_i$	A_{1b}, $10^{-5}\,K^{-1}$	A_{2b}, $10^{-8}\,K^{-2}$	A_{3b}, $10^{-9}\,K^{-3}$	A_{4b}, $10^{-11}\,K^{-4}$
	−5.33829	−2.074	1.62589	1.5924
Expansion coefficients for $T \ge T_i$	A_{1u}, $10^{-5}\,K^{-1}$	A_{2u}, $10^{-8}\,K^{-2}$	A_{3u}, $10^{-9}\,K^{-3}$	A_{4u}, $10^{-11}\,K^{-4}$
	−5.68261	17.62	−11.1076	15.8229

efficiency dependences [28]. For the crystal temperature $T \le T_i$, the incident extraordinary light wave with the wave vector $\mathbf{k}_e$ (Figure 2, *a*) will have a constant amplitude E^m_{ie}. Using the known approach [33], equations describing the evolution of the diffracted ordinary wave amplitudes $E^m_{dro}(y)$ and $E^m_{dlo}(y)$ with the vectors $\mathbf{k}_{or}$ and $\mathbf{k}_{ol}$, respectively, may be derived as

$$\frac{dE^m_{dro}}{dy} = -i\,\frac{\pi}{2\lambda}\,\frac{\Delta\varepsilon^{1m}_{13}}{n_o\cos\theta_{or}}\,E^m_{ie}\exp(i\Delta k^b_r y), \tag{4}$$

$$\frac{dE^m_{dlo}}{dy} = -i\,\frac{\pi}{2\lambda}\,\frac{\Delta\varepsilon^{1m}_{13}}{n_o\cos\theta_{ol}}\,E^m_{ie}\exp(i\Delta k^b_l y), \tag{5}$$

where $\Delta\varepsilon^{1m}_{13}$ — is the amplitude of the first spatial harmonic of dielectric tensor component disturbances by the RDS domain walls, and wave detuning depending on the crystal temperature and induced by the Bragg conditions at $\theta_{ol} = -\theta_{or}$, when $\mathbf{k}_e \perp \mathbf{K}$, are defined as follows:

$$\Delta k^b_l(T) = \Delta k^b_r(T) = \Delta k^b(T) \approx \frac{\pi\lambda}{n_o\Lambda^2}\left[1 - 2n_o\delta n_b(T)\,\frac{\Lambda^2}{\lambda^2}\right]. \tag{6}$$

Thus, in case of symmetric tuning ($\theta_{ol} = -\theta_{or}$, $\mathbf{k}_e \perp \mathbf{K}$), the diffraction efficiencies η_{eol} and η_{eor} of the doubly degenerate anisotropic Bragg diffraction for the left and right peaks shall be identical and their temperature dependence for $T \le T_i$ defined by wave detuning (6) may be derived from (4) or (5) as

$$\eta_{eol}(T) = \eta_{eor}(T) = \eta^m_{eo}\,\frac{\sin^2\left[\Delta k^b(T)d_{\text{ef}}/2\right]}{\left[\Delta k^b(T)d_{\text{ef}}/2\right]^2} \tag{7}$$

with the following maximum value:

$$\eta^m_{eo} = \left(\frac{\pi|\Delta\varepsilon^{1m}_{13}|d_{\text{ef}}}{2\lambda n_o\cos\theta_o}\right)^2. \tag{8}$$

This approach to the analysis of the temperature dependence of the doubly degenerate anisotropic Bragg diffraction efficiency on the RDS domain walls with the ordinary probing beam implemented for $T \ge T_i$ (see the vector diagram in Figure 2, *b*) made it possible to derive the following relations:

$$\Delta k^u_l(T) = \Delta k^u_r(T) = \Delta k^u(T) \approx \frac{\pi\lambda}{n_e\Lambda^2}\left[1 + 2n_e\delta n_u(T)\,\frac{\Lambda^2}{\lambda^2}\right], \tag{9}$$

$$\eta_{oel}(T) = \eta_{oer}(T) = \eta^m_{oe}\,\frac{\sin^2\left[\Delta k^u(T)d_{\text{ef}}/2\right]}{\left[\Delta k^u(T)d_{\text{ef}}/2\right]^2}, \tag{10}$$

$$\eta^m_{oe} = \left(\frac{\pi|\Delta\varepsilon^{1m}_{13}|d_{\text{ef}}}{2\lambda n_e\cos\theta_e}\right)^2. \tag{11}$$

Calculations of the temperature dependences of the doubly degenerate anisotropic Bragg diffraction efficiency on the RDS domain walls shown as solid curves in Figure 4 used relations (7), (6) and (3) for $T \le T_i$ and (10), (9) and (3) for $T \ge T_i$, where the maximum diffraction efficiencies η^m_{eo} and η^m_{oe} were assumed equal to $1.07 \cdot 10^{-3}$ and $1.18 \cdot 10^{-3}$, respectively. The temperature dependence of the ordinary and extraordinary refractive indices in equations (6) and (9) was ignored and they were replaced by an approximate value $n_o \approx n_e \approx 2.175$.

Comparison o the experimental data shown in Figure 4 with the calculated curves shows that they agree satisfactorily with each other within the addressed model of the doubly degenerate anisotropic Bragg diffraction on the RDS domain walls. The observed differences may be associated with the experimental errors as well as with the errors of the probing beam wave vector orientation ($\mathbf{k}_e$ or $\mathbf{k}_o$) with respect to the vector $\mathbf{K}$ of the RDS lattice and the sample's crystallographic axes. From the found η^m_{eo} and η^m_{oe} and equations (8) and (11), respectively, the disturbance amplitudes were estimated as $|\Delta\varepsilon^{1m}_{13}| = 1.55 \cdot 10^{-5}$ for $T \le T_i$ and $|\Delta\varepsilon^{1m}_{13}| = 1.63 \cdot 10^{-5}$ for $T \ge T_i$.

Amplitude of the first spatial harmonic $\Delta\varepsilon^{1m}_{13}$ is defined first by the maximum disturbance $\Delta\varepsilon^{\max}_{13}$ induced by an individual RDS domain walls due to the flexoelectric effect. This maximum value may be derived from the relations given in [26,27] as

$$\Delta\varepsilon^{\max}_{13} = n^2_o n^2_e\,\frac{P_S}{2\omega_0} \times \left|\frac{f_{1132}(p_{44}C^p_{14} - p_{41}C^p_{44}) + f_{3131}(p_{41}C^p_{14} - p_{44}C^p_{66})}{C^p_{44}C^p_{66} - (C^p_{14})^2}\right|, \tag{12}$$

where C^p_{mn} and p_{mn} — are the moduli of elasticity with constant electric polarization and elastic-optical coefficients of crystal in matrix notation; P_S — is the spontaneous polarization; ω_0 — is the domain wall half-thickness. Second, $\Delta\varepsilon^{1m}_{13}$ will depend on the ratio between h_i and $h_p = \Lambda - h_i$, respectively, for the original and repolarized crystal regions in RDS. Write the disturbances $\Delta\varepsilon_{13}(x) = \Delta\varepsilon_{31}(x)$ on the

spatial period Λ for the studied RDS with $\omega_0 \ll \Lambda$ considering the relations for individual walls [26,27] separating the original and repolarized regions as:

$$\Delta\varepsilon_{13}(x) = \Delta\varepsilon_{31}(x) = \Delta\varepsilon_{13}^{\max}\left\{\mathrm{ch}^{-2}\left[\frac{x+\Lambda/4+\Delta/4}{\omega_0}\right] - \mathrm{ch}^{-2}\left[\frac{x-\Lambda/4-\Delta/4}{\omega_0}\right]\right\}, \quad (13)$$

where $\Delta = h_i - h_p$. Numerical calculations of the complex amplitude of the first spatial harmonic using (13) have shown that, for the domain wall half-thicknesses in the range from 2 nm to 100 nm, it may be closely approximated as

$$\Delta\varepsilon_{13}^{1m} = i\,\frac{4\omega_0}{\Lambda}\,\Delta\varepsilon_{13}^{\max}\cos\left(\frac{\pi\Delta}{2\Lambda}\right). \quad (14)$$

In this case, as follows from (12), the disturbance amplitude $\Delta\varepsilon_{13}^{1m}$ does not depend on an unknown domain wall parameter ω_0 and its module may be written as

$$|\Delta\varepsilon_{13}^{1m}| = \frac{2n_o^2 n_e^2 P_S}{\Lambda}\cos\left(\frac{\pi\Delta}{2\Lambda}\right)|b_1 f_{1132} + b_2 f_{3131}| \quad (15)$$

with the following coefficients:

$$b_1 = \frac{p_{44}C_{14}^p - p_{41}C_{44}^p}{C_{44}^p C_{66}^p - (C_{14}^p)^2}, \quad b_2 = \frac{p_{41}C_{14}^p - p_{44}C_{66}^p}{C_{44}^p C_{66}^p - (C_{14}^p)^2}. \quad (16)$$

To estimate possible values of the flexoelectric coupling tensor components f_{1132} and f_{3131} of the studied 1% MgO : $LiTaO_3$ crystal that define the efficiency of the observed anisotropic diffraction, use the known elastic-optical coefficients $p_{41} = 0.028$ and $p_{44} = 0.028$ [34] that allow a replacement $p_{41} = p_{44} = p$ in (16):

$$b_1 = p\,\frac{C_{14}^p - C_{44}^p}{C_{44}^p C_{66}^p - (C_{14}^p)^2}, \quad b_2 = p\,\frac{C_{14}^p - C_{66}^p}{C_{44}^p C_{66}^p - (C_{14}^p)^2}. \quad (17)$$

The moduli of elasticity with constant electric polarization for the lithium tantalate crystal may be calculated using its known constitutive parameters [35] as

$$C_{14}^p = -2.170 \cdot 10^{10}\ \mathrm{N/m^2},\ C_{44}^p = 1.152 \cdot 10^{11}\ \mathrm{N/m^2}$$

and

$$C_{66}^p = 9.925 \cdot 10^{11}\ \mathrm{H/m^2},$$

leading to the following coefficients

$$b_1 = -p \cdot 1.249 \cdot 10^{-11}\ \mathrm{m^2/N}$$

and

$$b_2 = -p \cdot 1.104 \cdot 10^{-11}\ \mathrm{m^2/N}.$$

The close values in equation (15) may be replaced by a mean value

$$b_{av} = |b_1 + b_2|/2 \approx p \cdot 1.2 \cdot 10^{-11}\ \mathrm{m^2/N}$$

and the sum of the flexoelectric coupling tensor components may be estimated as

$$|f_{1132} + f_{3131}| \approx \frac{\Lambda|\Delta\varepsilon_{13}^{1m}|}{2n_o^2 n_e^2 P_S \cos(\pi\Delta/2\Lambda) b_{av}}. \quad (18)$$

Using the spontaneous polarization $P_S = 0.5\,\mathrm{C/m^2}$ [36] and other constitutive parameters of the lithium tantalate given above, and the obtained experimental data, we find that $|f_{1132} + f_{3131}| \approx 18$ V. Note that this data don't contradict with the known theoretical estimates for the flexoelectric coupling tensor components $f_{ijkl} \sim 1-10$ V [37,38].

Thus, the presence of an isotropic point in the stoichiometric 1%MgO : $LiTaO_3$crystal makes it possible to implement the degenerate anisotropic diffraction effects on RDS formed in the crystal with extraordinary (for $T \le T_i$) and ordinary ($T \ge T_i$) probing beams. In the studied sample for RDS with non-sloping *Y*-type walls with $\Lambda = 7.99\,\mu$m, the efficiency peaks $\eta_{eo}^m \approx 1.1 \cdot 10^{-3}$ and $\eta_{oe}^m \approx 1.2 \cdot 10^{-3}$ of the doubly degenerate anisotropy diffraction for the probing beam with $\lambda = 632.8$ nm were observed at $T_{dgb} = 41.5°$C and $T_{dgu} = 91.5°$C, respectively, at which the difference of squared refractive indices may be estimated as

$$n_o^2(T_{dgb}) - n_e^2(T_{dgb}) = n_e^2(T_{dgu}) - n_o^2(T_{dgu}) = 6.27 \cdot 10^{-3}.$$

The calculations based on the weak coupling approximation for the doubly degenerate anisotropic Bragg diffraction efficiency and experimental data for η_{eo}^m and η_{oe}^m provided the estimate $|f_{1132} + f_{3131}| \approx 18$ V for the flexoelectric coupling tensor components of the studied lithium tantalate sample. Analysis of the experimental temperature dependences for the power of the probing beam with the polarization vector oriented at 45° to the *Z* axis, transmitted through the 1% MgO : $LiTaO_3$ crystal and crossed analyzer, the isotropic point temperature $T_i = 69.31°$C was determined and the birefringence behavior $\delta n_{b,u}(T) = n_o(T) - n_e(T)$ was approximated by power series expansions for $30°\mathrm{C} < T \le T_i$ and $T_i \le T < 110°$C, respectively.

Funding

The study was performed under the state assignment of the Ministry of Science and Higher Education of the Russian Federation for 2023–2025 (task FEWM-2023-0012).

Conflict of interest

The authors declare that they have no conflict of interest.

References

[1] P. Ferrari, S. Grilli, P. DeNatale. *Ferroelectric Crystals for Photonic Applications* (Springer-Verlag, Berlin–Heidelberg, 2014). DOI: 10.1007/978-3-642-41086-4

[2] F.J. Kontur, I. Dajani, Y. Lu, R.J. Knize. Optics Express, **15**, 12882 (2007). DOI: 10.1364/OE.15.01.012882
[3] S.P. Kovalev, G.Kh Kitaeva. Pisma v ZhETF **94**, 95 (2011) (in Russian). DOI: 10.1134/S0021364011140074
[4] A.N. Tuchak, G.N. Goltsman, G.Kh. Kitaeva, A.N. Penin, S.V. Seliverstov, M.I. Finkel, A.V. Shepelev, P.V. Yakunin. Pisma v ZhETF **96**, 97 (2012) (in Russian). DOI: 10.31857/S1234567820170048
[5] L.A. Rios, C.E. Minor, N.A. Barboza, R.S. Cudney. Opt. Express, **26**, 17591 (2018). DOI: 10.1364/OE.26.017591
[6] T. Ding, Y. Zheng, X. Chen. Opt. Lett., **44**, 1524 (2019). DOI: 10.1364/OL.44.001524
[7] P.A. Prudkovsky. Pisma v ZhETF, **111** (494) 2020) (in Russian). DOI: 10.31857/S123456782008011X
[8] P.A. Prudkovsky. Pisma v ZhETF, **116** (667) 2022) (in Russian). DOI: 10.31857/S1234567822220049
[9] B. Nandy, S.C. Kumar, M. Ebrahim-Zadeh. Optics Express, **30**, 16340 (2022). DOI: 10.1364/OE.456023
[10] W. Yao, L. Deng, Y. Tian, A. Chang, P. Wang, J. Chen, H. Tan, J. Gao. Optics Continuum, **1**, 547 (2022). DOI: 10.1364/OPTCON.445930
[11] I. Mhaouech, V. Coda, G. Montemezzani, M. Chauvet, L. Guilbert. Opt. Lett., **41**, 4174 (2016). DOI: 10.1364/OL.41.004174
[12] S.M. Shandarov, E.N. Savchenkov, M.V. Borodin, A.E. Mandel, A.R. Akhmatkhanov, V.Ya. Shur. Ferroelectrics, **542**, 58 (2019). DOI: 10.1080/00150193.2019.1574663
[13] R.L. Byer, J. Nonlinear. Opt. Phys. Mater., **6**, 549 (1997). DOI: 10.1142/S021886359700040X
[14] C. Bäumer, D. Berben, K. Buse, H. Hesse, J. Imbrock. Appl. Phys. Lett., **82**, 2248 (2003). DOI: 10.1063/1.1566100
[15] I. Shoji, Y. Iwamoto, Y. Kagami, Y. Furukawa. *Novel Optical Materials and Applications* (Optica Publishing Group, 2022), NoTh2E.3. DOI: 10.1364/noma.2022.noth2e.3
[16] W. Wen-Le, L. You-Wen, Z. Xiao-Qi. Chinese Phys. Lett., **25**, 4303 (2008). DOI: 10.1088/0256-307X/25/12/033
[17] H.H. Lim, S. Kurimura, T. Katagai, I. Shoji. Jap. J. Appl. Phys., **52**, 032601 (2013). DOI: 10.7567/JJAP.52.032601
[18] A.L. Aleksandrinsky, O.A. Gliko, I.I. Naumova, V.I. Pryalkin. Kvantovaya elektronika, **23** (657), 1996 (1996).(in Russian) DOI: 10.1070/QE1996v026n07ABEH000743
[19] S.M. Shandarov, A.E. Mandel, T.M. Akylbaev, M.V. Borodin, E.N. Savchenkov, S.V. Smirnov, A.R. Akhmatkhanov, V.Ya. Shur. J. of Physics: Conf. Series, **867**, 012017 (2017). DOI: 10.1088/1742-6596/867/1/012017
[20] S.M. Shandarov, A.E. Mandel, E.N. Savchenkov, M.V. Borodin, S.V. Smirnov, A.R. Atmatkhanov, V.Ya. Shur. *Gologrаfiya. Nauka i praktika: XVI mezhdunarodnaya konferentsiya HOLOEXPO 2017: Tezisy dokladov* (MGTU im. N.E. Baumana, M., 2017), s. 178 (in Russian).
[21] E.N. Savchenkov, S.M. Shandarov, S.V. Smirnov, A.A. Esin, A.R. Akhmatkhanov, V.Ya. Shur. Pisma v ZhETF, **110** (165) 2019) (in Russian). DOI: 10.1134/S0370274X19150050
[22] D.A. Gubinskaya, M.A. Fedyanina, E.N. Savchenkov. *XX Vserossiisky molodezhny Samarskii konkurs-konferentsiya nauchnykh rabot po optike i lazernoy fizike, posvyashchennyi 100-letiyu so dnya rozhdeniya N.G. Basova: sbornik trudov* (Trovant, M., 2022), s. 308 (in Russian).
[23] E.N. Savchenkov, S.M. Shandarov, A.V. Dubikov, D.E. Kuzmin, M.A. Fedyanina, D.A. Gubinskaya, V.Ya.Shur, A.R. Akhmatkhanov, M.A. Tchyvakova. *XI Mezhdunarodnaya konferentsiya po fotonike i informatsionnoy optike. Sbornik nauchnykh trudov* (NUYaU MIFI, M., 2022), s. 60 (in Russian).
[24] V.A. Zhirnov. ZhETF., **35**, 1175 (1958). (in Russian).
[25] E.A. Eliseev, A.N. Morozovska, M.D. Glinchuk, R. Blinc. Phys. Rev. B, **79**, 165433 (2009). DOI: 10.1103/PhysRevB.79.165433
[26] S.M. Shandarov, E.N. Savchenkov, N.I. Burimov, A.R. Akhmatkhanov, V.Ya. Shur. Laser Physics, **30**, 025401 (2020). DOI: 10.1088/1555-6611/ab5858
[27] S.M. Shandarov, A.E. Mandel, S.V. Smirnov, T.M. Akylbaev, M.V. Borodin, A.R. Akhmatkhanov, V.Ya. Shur. Ferroelectrics. **496** (1), 134 (2016). DOI: 10.1080/00150193.2016.1157439
[28] V.I. Balakshii, V.N. Parygin, L.E. Chirkov. *Fizicheskie osnovy akustooptiki* (Radio i svyaz', M., 1985) (in Russian).
[29] J. Xu, R. Stroud. *Acousto-optic devices: principles, design, and applications* (Wiley, 1992).
[30] A.W. Warner, D.L. White, W.A. Bonner. J. Appl. Phys., **43**, 4489 (1972). DOI: 10.1063/1.1660950
[31] V.B. Voloshinov, V.N. Parygin, L.E. Tchirkov. Vestn. Mosk.un-ta. Ser. 3. Fiz., astr.., **17**, 305 (1976) (in Russian).
[32] V.Ya. Shur, A.R. Akhmatkhanov, I.S. Baturin. Appl. Phys. Rev., **2**, 040604 (2015). DOI: 10.1063/1.4928591
[33] L.N. Magdich, V.Ya. Molchanov. *Akustoopticheskie ustroistva i ikh primenenie* (Sovetskoe radio, M., 1978) (in Russian).
[34] L.P. Avakyants, D.F. Kiselev, N.N. Shchitov. FTT **18**, 2129 (1976) (in Russian).
[35] R.T. Smith, F.S. Welsh. J. Appl. Phys., **42**, 2219 (1971).
[36] A.M. Glass. Phys. Rev., **172**, 564 (1968).
[37] P. Zubko, G. Catalan, A.K. Tagantsev. Annu. Rev. Mater. Res., **43**, 387 (2013). DOI: 10.1146/annurev-matsci-071312-121634
[38] P.V. Yudin, A.K. Tagantsev. Nanotechnology, **24**, 432001 (2013). DOI: 10.1088/0957-4484/24/43/432001

Translated by E.Ilinskaya